Time-Domain Near-Field Analysis of Short-Pulse Antennas—Part I: Spherical Wave (Multipole) Expansion

Amir Shlivinski and E. Heyman, *Senior Member, IEEE*

***Abstract*—The radiation from a time-dependent source distribution in free-space is analyzed using time-domain (TD) spherical wave (multipole) expansion. The multipole moment functions are calculated from the time-dependent source distribution. The series convergence rate in the near and far zone and the bounds on the near-zone reactive field are determined as functions of the source support and of the pulse length. The formulation involves a spherical transmission line representation that can be extended to more general spherical configurations. This formulation also describes the field and energy transmission mechanisms in a physically transparent fashion that will be used in a companion paper to define and explore fundamental concepts such as TD reactive energy and Q and to derive bounds on the antenna properties. Finally, the concepts discussed above are demonstrated numerically for pulsed radiation by a circular current disk.**

***Index Terms*—Antenna theory, near field, short-pulse electromagnetics, time-domain analysis.**

I. Introduction

THIS work is concerned with the analysis of radiation from time-dependent source distributions directly in the time-domain (TD). The slant is toward the analysis of the near-field properties of short-pulse antennas, including the definition of fundamental concepts such as reactive power and energy, and the derivation of bounds of the antenna properties. In the present paper, we mainly consider new expressions for the field solutions while the energy properties and bounds will be considered in a companion paper [1]. The analysis in these papers is based on a systematic time-dependent spherical wave expansion and a spherical transmission line procedure that can readily be extended to more general spherical configurations.

One way of analyzing radiation from source distributions is by using Green's function integration. It is sometimes desirable, however, to express the field in a more transparent form, using basis functions that conform with the field structure in a particular space–time regime. The most common representations are the plane wave and the spherical wave expansions, which are frequently used in the frequency domain (FD). The TD plane wave approach has been used recently in [2] and [3] for the analysis of radiation from planar apertures and in [4] and [5] for radiation from volume source distributions. In [5], it has also been used to formulate a comprehensive TD "far-zone characterization" of antenna systems. The TD plane wave representation is based on a slant stack transform (SST) of the source distribution. It provides a physically transparent representation for the field in the radiation zone where the field is dominated by the *propagating* spectrum, but a complete spectral representation in the near zone must also involve the TD *evanescent* spectrum [4]. Another difficulty is that each spectral constituent is a *global* wave function and thereby noncausal. Although all noncausal contributions cancel each other in the overall spectral integration, this property complicates the physical interpretation [4].

The spherical wave expansion, on the other hand, consists only of strictly outgoing (causal) wave solutions. Furthermore, it provides a convenient framework for addressing the causal near to far zone transition, as each spherical wave combines both the propagating and the evanescent spectra. Spherical wave expressions have been used extensively in FD analysis of near-zone fields and of fundamental antenna limits [6]–[10]. More recently, the spherical wave expansion has been extended for radiation from time-dependent source distributions, using multipole expansion of the sources [11]–[14]. An alternative TD formulation has been used in [15] and [16] in connection with the near-field spherical scanning problem by expending the field in terms of decaying oscillations corresponding to the resonances of the measurement sphere.

In this two-part paper, we explore the antenna properties as implied by the TD spherical wave expansion. The formulation utilizes a TD spherical transmission line representation that describes the field and energy transmission mechanisms in a systematic and physically transparent fashion that can also be extended to more general spherical configurations. In the first part, we focus on the field solutions, while in the second part [1], we use this new expansion to explore the energy properties and to define fundamental TD concepts such as time-dependent reactive energy and the antenna Q. For time-harmonic fields, these concepts are well understood in terms of the stored energy [6]–[9], but they have to be redefined for short-pulse fields where there is no stored energy.

Concerning the layout of presentation, we start in Section II with the formulation of the TD spherical wave expansion in a general spherical configuration, identified by any conical cross section and stratification (Fig. 1). The derivation, which is outlined in the Appendix, is based on the spherical transmission line representation for time harmonic fields [17]. Then, in

Manuscript received September 30, 1997; revised May 4, 1998. This work was supported in part by the U.S. Air Force Office of Scientific Research under Grant 96-1-0039 and by the Israel Science Foundation under Grants 574/95 and 404/98.

The authors are with the Department of Electrical Engineering, Physical Electronics, Tel-Aviv University, Tel-Aviv, 69978 Israel.

Publisher Item Identifier S 0018-926X(99)03731-X.

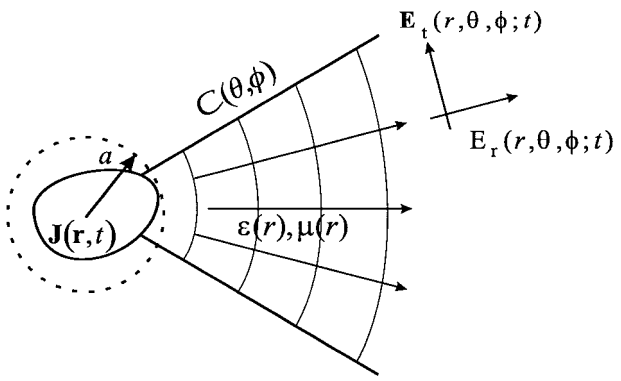

Fig. 1. A spherical transmission line.

Section III, the general formulation is applied for radiation in free-space. The radiated field is completely described by the "TD multipole moments," which are calculated in Section III-C directly from the time-dependent source distribution. The convergence properties and bounds on the near-zone reactive field are explored in Section III-D. Finally, the concepts mentioned above are demonstrated in Section IV for pulsed radiation by a circular current disk. In order to check the validity of the calculations, the multipole expansion of the TD radiation pattern is compared in Section IV-C with a closed-form expression obtained independently via the SST formulation of [5]. In [1], this example will be further studied from a reactive energy perspective.

II. Time-Domain Spherical Transmission Line Representation

Referring to Fig. 1, we consider first the propagation in a spherically stratified domain with $\epsilon(r)$ and $\mu(r)$, bounded by a perfectly conducting, general conical surface $\mathcal{C}(\theta, \phi)$. The spherical cross section bounded by $\mathcal{C}$ is termed $\mathcal{S}$. In Section III, we shall consider the special case of a homogeneous medium and unbounded spherical domain $\mathcal{S} = 4\pi$. The source distribution $\mathbf{J}(\mathbf{r}, t)$ is assumed to be confined in the region $r < a$ where we utilize the conventional spherical coordinate system $\mathbf{r} = (r, \theta, \phi)$.

In view of the problem symmetry, the field is decomposed into radial and transverse components

$$\mathbf{E}(\mathbf{r}, t) = \mathbf{E}_t + \hat{\mathbf{r}} E_r, \qquad \mathbf{E}_t = \hat{\boldsymbol{\theta}} E_\theta + \hat{\boldsymbol{\phi}} E_\phi \tag{1}$$

where the carets are used to denote unit vectors. The field may be decomposed into E- and H-type modes denoted, respectively, by superscript e and h. As discussed in the Appendix, the expansion has the form

$$\mathbf{E}_t(\mathbf{r}, t) = \frac{1}{r} \sum_{\alpha,\nu} V_\nu^\alpha \mathbf{e}_\nu^\alpha,$$

$$E_r(\mathbf{r}, t) = \frac{\eta c}{r^2} \sum_{\nu} k_{t\nu}^e \Phi_\nu^e \partial_t^{-1} I_\nu^e \tag{2a}$$

$$\mathbf{H}_t(\mathbf{r}, t) = \frac{1}{r} \sum_{\alpha,\nu} I_\nu^\alpha \mathbf{h}_\nu^\alpha$$

$$H_r(\mathbf{r}, t) = \frac{\eta^{-1} c}{r^2} \sum_{\nu} k_{t\nu}^h \Phi_\nu^h \partial_t^{-1} V_\nu^h \tag{2b}$$

where $\partial_t^{-1} \equiv \int_{-\infty}^t dt$, $c(r) = 1/\sqrt{\epsilon\mu}$, and $\eta(r) = \sqrt{\mu/\epsilon}$. Here, $\Phi_\nu^\alpha(\theta, \phi)$, $\mathbf{e}_\nu^\alpha(\theta, \phi)$, and $\mathbf{h}_\nu^\alpha(\theta, \phi)$ are the transversal scalar and vector mode functions which depend only on $\mathcal{S}$ and are independent of (r, t), while ν denotes the mode index and $\alpha = e$ or h (see Section II-A). Note that the summation for $\mathbf{E}_t$ and $\mathbf{H}_t$ involve all modes (ν) of both types ($\alpha = e, h$), while the summations for E_r and H_r involve only E or H modes, respectively. In (2), $V_\nu^\alpha(r, t)$ and $I_\nu^\alpha(r, t)$ are the modal amplitude functions which depend only on (r, t) as described by the time-dependent radial transmission line in Section III-B. Also, for simplicity, (2b) is written only for $r > a$ (outside the source domain).

A. Spherical Mode Functions

The modal fields are determined by the scalar eigenvalue problem

$$\left(\nabla_t^2 + k_{t\nu}^{\alpha 2}\right) \Phi_\nu^\alpha(\theta, \phi) = 0 \qquad \text{in } \mathcal{S} \tag{3}$$

with the boundary conditions $\Phi_\nu^e|_{\mathcal{C}} = 0$ and $\partial_n \Phi_\nu^h|_{\mathcal{C}} = 0$, where n is the coordinate normal to $\mathcal{C}$ and $\nabla_t^2 \equiv (\sin\theta)^{-1}\partial_\theta \sin\theta\, \partial_\theta + (\sin\theta)^{-2}\partial_\phi^2$. Here Φ_ν^α, $k_{t\nu}^\alpha$ are the eigenfunctions and eigenvalues, ν is the mode index and $\alpha = e$ or h. For $k_{t\nu}^e = 0$ (TEM mode), the boundary condition above is replaced by $\Phi_\nu^e|_{\mathcal{C}} =$ constant.

The transverse vector eigenfunctions $\mathbf{e}_\nu^\alpha$ and $\mathbf{h}_\nu^\alpha \equiv \hat{\mathbf{r}} \times \mathbf{e}_\nu^\alpha$ are found from Φ_ν^α via

$$\mathbf{e}_\nu^e = -(k_{t\nu}^e)^{-1} {}_t\nabla \Phi_\nu^e, \qquad \mathbf{h}_\nu^h = -(k_{t\nu}^h)^{-1} {}_t\nabla \Phi_\nu^h \tag{4}$$

where ${}_t\nabla \equiv \hat{\boldsymbol{\theta}}\partial_\theta + \hat{\boldsymbol{\phi}}(\sin\theta)^{-1}\partial_\phi$ (note that our definition of ${}_t\nabla$ and ∇_t^2 differ from those in [17, sec. 2.5] by a factor r). The scalar eigenfunctions may be normalized to obtain a *real orthonormal* set. From the definition in (4), the vector eigenfunctions are also orthonormal, with

$$\oiint_{\mathcal{S}} d\Omega\, \Phi_\nu^\alpha \Phi_{\nu'}^{\alpha'} = \oiint_{\mathcal{S}} d\Omega\, \mathbf{e}_\nu^\alpha \cdot \mathbf{e}_{\nu'}^{\alpha'} = \delta_{\nu,\nu'}\delta_{\alpha,\alpha'} \tag{5}$$

where $d\Omega = \sin\theta\, d\theta\, d\phi$ and $\delta_{i,i'}$ is the Kronecker delta.

B. The Time-Dependent Radial Wave Equations

The mode amplitudes in (2) are described by radial wave equations which are independent of (θ, ϕ). There are two principal modes functions: $I_\nu^e(r, t)$ for the E modes and $V_\nu^h(r, t)$ for the H modes, which are governed by [cf. (38)]

$$\left[\epsilon \frac{\partial}{\partial r} \epsilon^{-1} \frac{\partial}{\partial r} - \frac{1}{c^2}\frac{\partial^2}{\partial t^2} - \frac{k_{t\nu}^{e2}}{r^2}\right] I_\nu^e = \epsilon \frac{\partial}{\partial t} v_\nu^e - \epsilon \frac{\partial}{\partial r} \frac{i_\nu^e}{\epsilon} \tag{6a}$$

$$\left[\mu \frac{\partial}{\partial r} \mu^{-1} \frac{\partial}{\partial r} - \frac{1}{c^2}\frac{\partial^2}{\partial t^2} - \frac{k_{t\nu}^{h2}}{r^2}\right] V_\nu^h = \mu \frac{\partial}{\partial t} i_\nu^h \tag{6b}$$

where $k_{t\nu}^\alpha$ are the eigenvalues of (3). Having found these principal mode amplitudes, the associate amplitudes $V_\nu^e(r, t)$ and $I_\nu^h(r, t)$ are calculated via [cf. (39)]

$$\begin{Bmatrix} V_\nu^e \\ I_\nu^h \end{Bmatrix} = -c\eta^{\pm 1} \partial_t^{-1} \begin{Bmatrix} \partial_r I_\nu^e + i_\nu^e \\ \partial_r V_\nu^h \end{Bmatrix}. \tag{7}$$

In the above, $v_\nu^\alpha(r,t)$ and $i_\nu^\alpha(r,t)$ are the transmission line sources. They are calculated by projecting $\mathbf{J}(\mathbf{r},t)$ onto the mode functions via

$$v_\nu^e(r,t) = -\eta c k_{t\nu}^e \partial_t^{-1} \oiint d\Omega\, J_r(\mathbf{r},t)\Phi_\nu^e(\theta,\phi)$$

$$v_\nu^h \equiv 0 \tag{8a}$$

$$i_\nu^\alpha(r,t) = r \oiint d\Omega\, \mathbf{J}(\mathbf{r},t)\cdot \mathbf{e}_\nu^\alpha(\theta,\phi)$$

$$\text{for } \alpha = e \text{ or } h. \tag{8b}$$

III. Free-Space Solution: Spherical Waves and Multipole Moments

A. Spherical Mode Functions

From here on we consider radiation in free-space only. For an unbounded spherical domain, the normalized scalar eigenfunctions and eigenvalues of (3) are

$$\Phi_\nu^\alpha(\theta,\phi) = Y_{nm}^{(s)}(\theta,\phi), \qquad k_{t\nu}^\alpha = \sqrt{n(n+1)} \tag{9}$$

where ν is a triple index $\nu = (n,m,s)$, $s = 1,2$, $n = 0,1,\cdots,$, and $0 \le m \le n$. $Y_{nm}^{(s)}$ are the *real* spherical harmonics

$$\begin{Bmatrix} Y_{nm}^{(1)} \\ Y_{nm}^{(2)} \end{Bmatrix} = y_{nm} P_n^m(\cos\theta) \begin{Bmatrix} \cos \\ \sin \end{Bmatrix} m\phi$$

$$y_{nm} = \sqrt{\varepsilon_m \frac{2n+1}{4\pi}\frac{(n-m)!}{(n+m)!}} \tag{10}$$

with $P_n^m(x)$ being the associate Legendre functions [18, ch. 8] and $\varepsilon_m = 1$ or 2 for $m = 0$ or $m \ge 1$, respectively. From (4), the orthonormal vector mode functions are given by

$$\mathbf{e}_\nu^e = \mathbf{h}_\nu^h = \frac{y_{nm}}{\sqrt{n(n+1)}} \left[\hat{\boldsymbol{\theta}} P_n'^m(\cos\theta)\sin\theta \begin{Bmatrix} \cos \\ \sin \end{Bmatrix} m\phi + \hat{\boldsymbol{\phi}} \frac{m}{\sin\theta} P_n^m(\cos\theta) \begin{Bmatrix} \sin \\ -\cos \end{Bmatrix} m\phi \right] \tag{11}$$

while $\mathbf{e}_\nu^h = -\mathbf{h}_\nu^e$ are obtained by replacing in (11) $\hat{\boldsymbol{\theta}} \to -\hat{\boldsymbol{\phi}}$ and $\hat{\boldsymbol{\phi}} \to \hat{\boldsymbol{\theta}}$. Here $P_n'^m(x) \equiv (\partial/\partial x)P_n^m(x)$ and the upper and lower cases are for $s = 1,2$, respectively. The set of scalar and vector spherical harmonics satisfy the orthogonality condition (5) with respect to the indexes α, n, m, s, and are also complete: $\sum_{n,m,s} Y_{mn}^{(s)}(\hat{\mathbf{r}}) Y_{mn}^{(s)}(\hat{\mathbf{r}}') = \delta(\hat{\mathbf{r}} - \hat{\mathbf{r}}')$.

B. The Mode Amplitude Solutions

From (6) with (9), the wave equations for $I_\nu^e(r,t)$ and $V_\nu^h(r,t)$ are

$$\left[\frac{\partial^2}{\partial r^2} - \frac{1}{c^2}\frac{\partial^2}{\partial t^2} - \frac{n(n+1)}{r^2}\right] \begin{Bmatrix} I_\nu^e \\ V_\nu^h \end{Bmatrix} = \begin{Bmatrix} -\dfrac{\partial}{\partial r} i_\nu^e + \epsilon \dfrac{\partial}{\partial t} v_\nu^e \\ \mu \dfrac{\partial}{\partial t} i_\nu^h \end{Bmatrix}. \tag{12}$$

Outside the source region, for $r > a$, the solution of (12) can be expressed as

$$\begin{Bmatrix} I_\nu^e(r,t) \\ V_\nu^h(r,t) \end{Bmatrix} = \mathcal{L}_n^{(1)} M_\nu^\alpha(\tau), \qquad \tau \equiv t - r/c \tag{13}$$

where the $\mathcal{L}_n^{(1)}$ have either one of the following alternative forms:

$$\mathcal{L}_n^{(1)} = \sum_{l=0}^{n} a_{n,l} \left(\frac{c}{r}\right)^l \partial_t^{-l} \tag{14}$$

where $a_{n,l} = 2^{-l}((n+l)!)/(l!(n-l)!)$. The "TD multipole moments" $M_\nu^\alpha(t)$ are obtained from the transmission-line sources v_n^α and i_ν^α. Expressions for $M_\nu^\alpha(t)$ *directly* in terms of $\mathbf{J}(\mathbf{r},t)$ are given in (22) below.

From the series solution in (14) one observes that only the $l = 0$ terms are propagating with pure delay and without distortion, i.e., they are proportional to $M_\nu^\alpha(\tau)$. The large l terms, on the other hand, decay like r^{-l}, leaving the far-zone field dominated by the $l = 0$ terms. The high-order terms dominate in the near zone where they contribute to the "TD reactive energy." The role of these constituents will be defined and explored in Part II [1].

Having found I_ν^e and V_ν^h, the associate solutions V_ν^e and I_ν^h outside the source domain are calculated via (7), giving

$$\begin{Bmatrix} V_\nu^e(r,t) \\ I_\nu^h(r,t) \end{Bmatrix} = \eta^{\pm 1} \mathcal{L}_n^{(2)} M_\nu^\alpha(\tau), \qquad \alpha = e \text{ or } h \tag{15}$$

where

$$\mathcal{L}_n^{(2)} = \sum_{l=0}^{n+1} b_{n,l} \left(\frac{c}{r}\right)^l \partial_t^{-l} \tag{16}$$

with $b_{n,l} = a_{n,l} + (l-1)a_{n,l-1}$ for $0 \le l \le n+1$ (note that $b_{n,0} = a_{n,0} = 1$ and $b_{n,n+1} = n a_{n,n}$).

The final expressions for the TD field are obtained by substituting (13) and (15) in (2), giving

$$\mathbf{E}_t(\mathbf{r},t) = \frac{\eta}{r}\sum_\nu \mathbf{e}_\nu^e(\theta,\phi)\mathcal{L}_n^{(2)} M_\nu^e(\tau) + \frac{1}{r}\sum_\nu \mathbf{e}_\nu^h(\theta,\phi)\mathcal{L}_n^{(1)} M_\nu^h(\tau) \tag{17a}$$

$$E_r(\mathbf{r},t) = \frac{\eta c}{r^2}\sum_\nu \sqrt{n(n+1)}\Phi_\nu(\theta,\phi)\partial_t^{-1}\mathcal{L}_n^{(1)} M_\nu^e(\tau) \tag{17b}$$

with similar expressions for $\mathbf{H}$. A slightly modified representation, which may be more convenient in numerical calculations, is obtained by noting that $M_\nu^\alpha(t)$ can be expressed as [see (22) below]

$$M_\nu^e(t) = \partial_t^{N^\alpha} m_\nu^e(t) \tag{18}$$

where $N^\alpha = n$ or $n+1$ for $\alpha = e$ or h. Expressions (17) can be rewritten now as

$$\mathbf{E}_t(\mathbf{r},t) = \frac{\eta}{r}\sum_\nu \mathbf{e}_\nu^e(\theta,\phi)\hat{\mathcal{L}}_n^{(2)} m_\nu^e(\tau) + \frac{1}{r}\sum_\nu \mathbf{e}_\nu^h(\theta,\phi)\hat{\mathcal{L}}_n^{(1)} m_\nu^h(\tau) \tag{19a}$$

$$E_r(\mathbf{r},t) = \frac{\eta c}{r^2}\sum_\nu \sqrt{n(n+1)}\Phi_\nu(\theta,\phi)\partial_t^{-2}\hat{\mathcal{L}}_n^{(1)} m_\nu^e(\tau) \tag{19b}$$

where the integral operators $\mathcal{L}_n^{(1,2)}$ of (14) and (15) are now replaced by the differential operators $\hat{\mathcal{L}}_n^{(1)} = \sum_{l=0}^{n} a_{n,l}(c/r)^l \partial_t^{n+1-l}$ and $\hat{\mathcal{L}}_n^{(2)} = \sum_{l=0}^{n+1} b_{n,l}(c/r)^l \partial_t^{n-l}$ operating on $m_\nu^\alpha(t)$.

Finally, as indicated above, the far-zone field is dominated by the $l = 0$ term in $\mathcal{L}_n^{(1,2)}$, giving $\mathcal{L}_n^{(1,2)} \sim 1$. Thus, the far-zone field has the form

$$\mathbf{E}(\mathbf{r}, t) \sim r^{-1}\mathbf{F}(t - r/c, \hat{\mathbf{r}}) \tag{20}$$

where the "TD radiation pattern" $\mathbf{F}$ is given by

$$\mathbf{F}(t, \hat{\mathbf{r}}) = \eta \sum_\nu \mathbf{e}_\nu^e(\theta, \phi) M_\nu^e(t) + \sum_\nu \mathbf{e}_\nu^h(\theta, \phi) M_\nu^h(t). \tag{21}$$

Note that $\mathbf{F}$ can also be calculated via the slant stack transform (SST) of $\mathbf{J}(\mathbf{r}, t)$ (see [5] and also (34) below).

C. The Time-Domain Multipole Moments

The expressions for calculating the TD multipole moments from $\mathbf{J}(\mathbf{r}, t)$ can be derived via the TD transmission line procedure as described after (14). Alternatively, they may be derived via the frequency-domain analysis in the Appendix. The result is

$$M_\nu^e(t) = \frac{-1}{2n!}\partial_t^n \iiint_V dV \left(\frac{r}{2c}\right)^n \mathbf{h}_\nu^e \cdot \int_{-1}^{1} d\xi (1-\xi^2)^n \nabla \times \mathbf{J}(\mathbf{r}, t + \xi r/c') \tag{22a}$$

$$M_\nu^h(t) = \frac{\eta/c}{2n!}\partial_t^{n+1} \iiint_V dV \left(\frac{r}{2c}\right)^n \mathbf{e}_\nu^h \cdot \int_{-1}^{1} d\xi (1-\xi^2)^n \mathbf{J}(\mathbf{r}, t + \xi r/c) \tag{22b}$$

[in (22a) the ∇ operates only on the $\mathbf{r}$ variable in $\mathbf{J}$]. The functions m_ν^α of (18) are defined by the same integrals but without the derivatives $\partial_t^{N^\alpha}$.

Equation (22), should be understood as follows. First, for source points on any spherical shell of radius r, the ξ integration represents a local temporal average of the current in the time window $t \pm r/c$. Next, the time-averaged source distribution on each spherical shell r is projected onto the basis functions $\mathbf{h}_\nu^e$ and $\mathbf{e}_\nu^h$ via the angular (Ω) integration and, finally, the result is integrated as a function of r. Note that for the large n the main contribution comes from sources close to the external boundary ($r \simeq a$).

The TD multipole functions may also be found by measuring the radiated field on any sphere. Specifically, from (21) they may be found from the TD radiation pattern via

$$M_\nu^e(t) = \eta^{-1} \oiint d\Omega\, \mathbf{e}_\nu^e \cdot \mathbf{F}(t, \hat{\mathbf{r}})$$

$$M_\nu^h(t) = \oiint d\Omega\, \mathbf{e}_\nu^h \cdot \mathbf{F}(t, \hat{\mathbf{r}}). \tag{23}$$

D. Approximate Expressions and Series Convergence

In this section, we derive large n approximations for the TD multipole moments and, thus, establish the dominant field structure and the series convergence rate. The approximate expressions will also be use in [1] in connection with the bounds on the gain.

We first note that the effective width of the $(1-\xi^2)^n$ window in (22), henceforth termed ξ_n, can be quantified by

$$\xi_n = \left[\int_{-1}^{1} d\xi\, \xi^2 (1-\xi^2)^n\right]^{1/2} = \left[\frac{2(2n)!!}{(2n+3)!!}\right]^{1/2} \sim (\pi/4)^{1/4} n^{-(3/4)} \tag{24}$$

where $(2n)!! \equiv 2 \cdot 4 \cdots 2n \sim \sqrt{\pi}(2n)^{n+1/2}e^{-n}$ and $(2n+1)!! \equiv 1 \cdot 3 \cdots (2n+1) \sim \sqrt{2}(2n)^{n+1}e^{-n}$ (the large n approximations follow from Stirling's formula [18, eq. (6.1.37)]). For large n, $\xi_n \to 0$ so that $\mathbf{J}$ is approximately constant within the time window $t \pm \xi_n r/c$ and may be pulled out of the ξ integration in (22). This approximation is valid if $\xi_n r/c \ll T$, where T is a typical pulse length in $\mathbf{J}$. Applying this requirement for all $\mathbf{r} \in V$ we obtain

$$cT/a \gg \xi_n \sim (\pi/4)^{1/4} n^{-(3/4)}. \tag{25}$$

This sets a lower bound on the values of n for a given a and T, for which the analysis below applies.

Under the conditions above we may pull $\mathbf{J}$ out of the ξ integration in (22). Using $\int_{-1}^{1} d\xi (1-\xi^2)^n = (2^{n+1}n!)/((2n+1)!!)$ for the ξ integral we obtain

$$m_\nu^\alpha(t) \simeq \begin{Bmatrix} -1 \\ \eta/c \end{Bmatrix} \frac{c^{-n}}{(2n+1)!!} \int_0^a dr r^{n+2} p_\nu^\alpha(r, t) \tag{26}$$

where upper and lower signs correspond to $\alpha = e$ or h, respectively, and

$$p_\nu^e(r, t) = \oiint d\Omega\, \mathbf{h}_\nu^e \cdot \nabla \times \mathbf{J}(\mathbf{r}, t)$$

$$p_\nu^h(r, t) = \oiint d\Omega\, \mathbf{e}_\nu^h \cdot \mathbf{J}(\mathbf{r}, t). \tag{27}$$

The integration in (26) is bounded by $(n+3)^{-1}a^{n+3}p_{\nu_{\max}}^\alpha(t)$, where $p_{\nu_{\max}}^\alpha$ are bounds on $p_\nu^\alpha(r, t)$. Using also the Stirling formula for $(2n+1)!!$ we obtain

$$m_\nu^\alpha(t) \sim \begin{Bmatrix} -1 \\ \eta/c \end{Bmatrix} \frac{a^3}{2^{3/2}n(n+3)} \left(\frac{e}{2}\frac{a}{nc}\right)^n p_{\nu_{\max}}^\alpha(t). \tag{28}$$

Substituting (28) into (18) and using $\partial_t \sim O(T^{-1})$, where T is a typical pulselength of the source, one finds for large n that $M_\nu^\alpha \sim (a/ncT)^n$. The relevant terms in the series (21) for the radiation pattern $\mathbf{F}$ in are, therefore, of order

$$n \sim O(a/cT) \tag{29}$$

(see also numerical example in Section IV). Additional decay of the series is provided by $p_{\nu_{\max}}^\alpha(t)$ in (28), i.e., by the angular spectrum of the source, but it is not considered here.

Considering now the full-field solution in (17) [or (19)] one finds that a typical (n, l) term of the E or

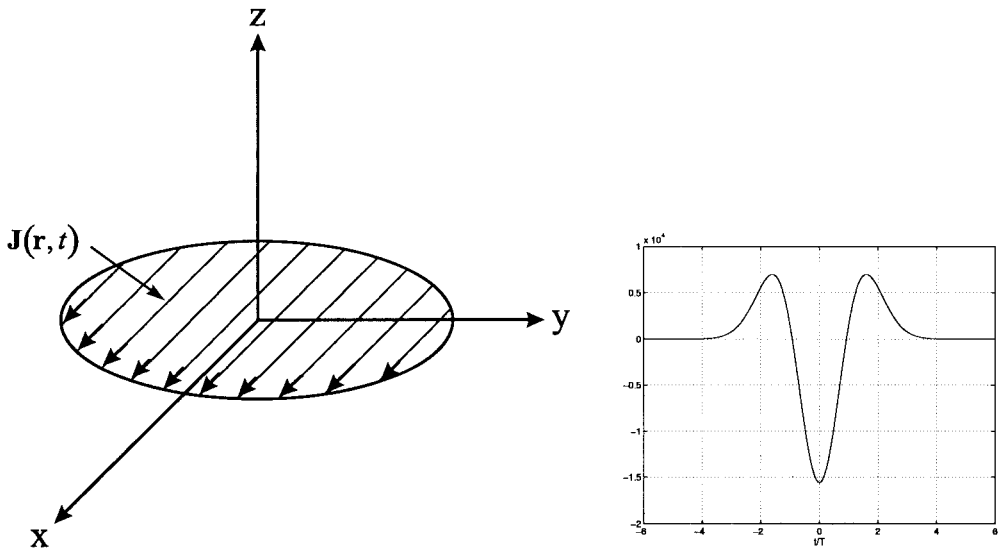

(a) (b)

Fig. 2. (a) Physical configuration for the numerical example. (b) The normalized excitation pulse.

H mode behaves like $(\eta/r)\mathbf{e}^e_\nu b_{n,l}(cT/r)^l T^{-n} m^e_\nu(t)$ or $(1/r)\mathbf{e}^h_\nu a_{n,l}(cT/r)^l T^{-n-1} m^h_\nu(t)$, respectively. For a given n, we may compare now the $l=0$ and 1 terms in the series. Recalling the expression for $a_{n,l}$ and $b_{n,l}$ in (14) and (16), we find that the $l=0$ term dominates only if $r/cT \gg n^2$. Thus, considering only the relevant n defined in (29) we conclude that the far-field approximation in (21) is valid for

$$r \gg a^2/cT \equiv F \tag{30}$$

where F is the TD Fresnel distance [20].

For small r, on the other hand, the full wave solution is dominated by the terms with the largest l. Noting from (14) and (16) that $a_{n,n} = (2n)!/2^n n! \simeq \sqrt{2}(2n/e)^n$ and $b_{n,n+1} = n a_{n,n}$ we find that modal fields in (17) [or (19)] are dominated by $\mathbf{E}^e \sim \mathbf{e}^e_\nu(\eta/r)2^{-1/2}((2/e)(nc/r))^{n+1} T m^e_\nu \simeq \mathbf{e}^e_\nu \eta (a/r)^{n+2} cT a[2e(n+3)]^{-1} p^e_{\nu_{\max}}$ and $\mathbf{E}^h \sim \mathbf{e}^h_\nu(1/r)2^{1/2}((2/e)(nc/r))^n T^{-1} m^h_\nu \simeq \mathbf{e}^h_\nu \eta (a/r)^{n+1}(a^2/cT)[2n(n+3)]^{-1} p^h_{\nu_{\max}}$, where we also used (28) for m^α_ν. Thus, the near-zone field of the large n modes is rapidly growing, but it is dominated by $(a/r)^{N^\alpha}$ and, hence, is bounded for all $r > a$.

IV. Example: Pulsed Radiations from a Circular Current Disk

The concepts above are demonstrate here for an example of a circular disk of radius a carrying a pulsed current (Fig. 2)

$$\mathbf{J}(\mathbf{r}, t) = \hat{\mathbf{x}}\delta(z) f(t), \qquad r < a \tag{31}$$

where $f(t)$ is an arbitrary pulse. Specifically, we shall use the twice differentiated Gaussian

$$f(t) = \left(3\gamma\sqrt{\pi/2}\right)^{-1/2} e^{-(t/\gamma)^2} H_2(t/\gamma) \tag{32}$$

where $H_2(x) = 4x^2 - 2$ is the Hermite polynomial of order 2. The constants in (32) were chosen so that $\int dt f^2(t) = 1$ and $\gamma = (12/7)^{1/2} T$ where $T = \int dt\, t^2 f^2(t)$ is the pulse length.

We shall calculate the TD multipole moments for both "small" and "large" disks identified by $a \simeq cT$ and $a \gg cT$, respectively, and shall explore the convergence as a function of the normalized disk size a/cT. The multipole expansion results will be verified by comparison with independent calculations for the far-zone field via the SST formulation of [5]. These multipole moments will also be used in Part II [1] to calculate the TD reactive energy and the Q of this source.

A. The Time-Domain Multipole Moments

Since the integrals in (22) are expressed in spherical coordinates, we first rewrite (31) as $\mathbf{J} = \hat{\mathbf{x}} r^{-1}\delta(\theta - \pi/2) f(t)$. Noting next for $\theta = \pi/2$ that $\hat{\mathbf{x}} = \hat{\mathbf{r}}\cos\phi - \hat{\boldsymbol{\phi}}\sin\phi$, it follows that (22) vanish for all m except for $m = 1$. Using also the values of $P^m_n(0)$ and $P'^m_n(0)$ from [18, eqs. (8.6.1), (8.6.3)], we finally obtain for the E modes with $m = 1$ that $M^e_\nu(t) = 0$ for $s = 2$ while for $s = 1$

$$M^e_\nu(t) = \frac{-1}{(2c)^n}\frac{\sqrt{n+1/2}}{n(n+1)!}\frac{\Gamma\left(\frac{n}{2}+1\right)}{\Gamma\left(\frac{n+1}{2}\right)}\cos((n+1)\pi/2) \times \int_0^a dr\, r^n \int_{-1}^1 d\xi (1-\xi^2)^n \times \left[(n+1)^2 f^{(n)}\left(t + \frac{\xi r}{c}\right) + \frac{\xi r}{c} f^{(n+1)}\left(t + \frac{\xi r}{c}\right)\right] \tag{33a}$$

where $f^{(n)} \equiv \partial^n_t f$. For the H modes with $m = 1$ we obtain $M^h_\nu(t) = 0$ for $s = 1$ while for $s = 2$

$$M^h_\nu(t) = \frac{\eta/c}{(2c)^n}\frac{\sqrt{n+1/2}}{n(n+1)!}\frac{\Gamma\left(\frac{n+3}{2}\right)}{\Gamma\left(\frac{n}{2}\right)}\sin((n+1)\pi/2) \times \int_0^a dr\, r^{n+1} \int_{-1}^1 d\xi (1-\xi^2)^n f^{(n+1)}\left(t + \frac{\xi r}{c}\right). \tag{33b}$$

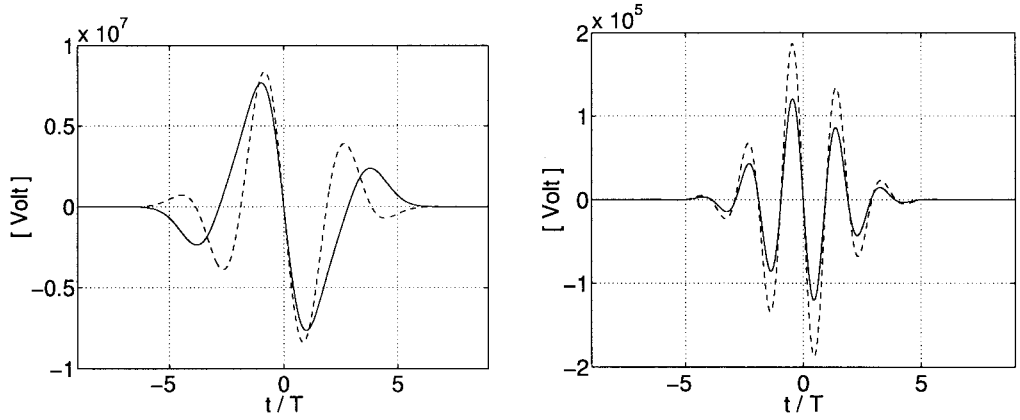

(a) (b)

Fig. 3. The time-dependent multipole moments $\eta\ M_\nu^e(t)$ (solid) and $M_\nu^h(t)$ (dashed) for a disk of radius $a = 3cT$ versus the normalized time t/T. (a) Low-order moments: $n = 1$ and 2 for the E and H mode, respectively. (b) Large-order moments: $n = 10$ and 11 for the H and E mode, respectively.

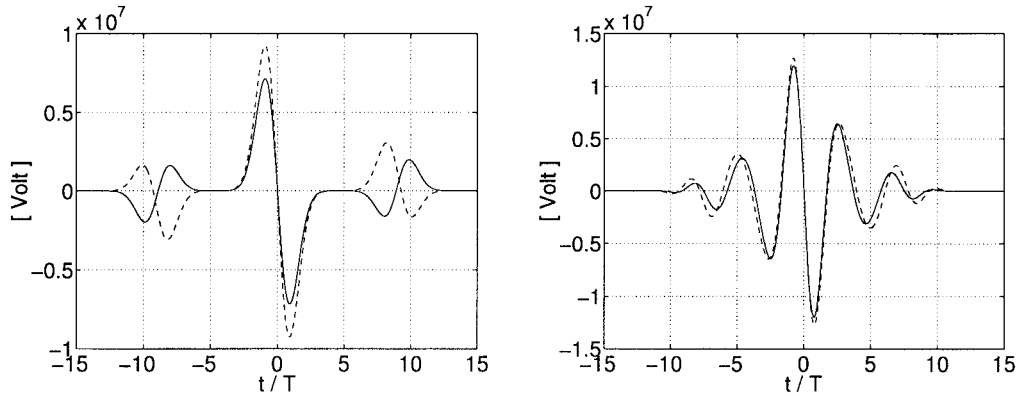

(a) (b)

Fig. 4. As in Fig. 3 for a disk of radius $a = 9cT$.

Note also that $M_\nu^{e,h}(t) = 0$ for even and odd values of n, respectively.

The integrals in (33) have been calculated numerically for $f(t)$ in (32). Examples for the resulting $M_\nu^\alpha(t)$ for a "small" and "large" disks with radii $a = 3cT$ and $9cT$, respectively, are shown in Figs. 3 and 4, respectively. Each figure shows examples for both low- and high-order modes. Note that for the small disk case, the higher order modes are weakly excited as predicted in (28) and (29). In [1] this observation will be further quantified using energy considerations.

B. Field Calculations

Next we calculate the field via (17). The results are checked by comparing the TD radiation pattern obtained via (21) with the closed-form expression obtained independently via the STT [see (35)–(37)]. Both results are available for all (θ, ϕ), but we only show here the waveforms for $\theta = 0$. Using the limiting values of the spherical basis functions (11) from [9, eq. (A1.7.3)], we obtain for $m = 1$ and $s = 1, 2$: $\mathbf{e}_\nu^e|_{\theta=0} = -(1/2)\sqrt{(n+(1/2))\pi}\{\hat{\mathbf{x}};\ \hat{\mathbf{y}}\}$. $\mathbf{e}_\nu^h|_{\theta=0}$ is given by replacing in this expression $\{\hat{\mathbf{x}};\ \hat{\mathbf{y}}\} \rightarrow \{-\hat{\mathbf{y}};\ \hat{\mathbf{x}}\}$.

Fig. 5 shows the radiation pattern at $\theta = 0$ for disks of radii $a = 3cT$ and $9cT$. For each case, the figure compares the "exact" SST result (37) to the mode summation result obtained by summing n terms with $n = a/cT$ and $2a/cT$. Note that the number of modes needed is essentially $n \sim 3(a/cT)$. Next, Fig. 6 depicts the field along the z axis for the disk $a = 9cT$ for which the Fresnel distance (30) is given by $F \simeq a^2/cT = 9a$. The results are shown at three ranges: $z = 3a$, $9a$, and $18a$ (i.e., in the near, intermediate, and far zones, respectively).

C. The Radiation Pattern via the Slant Stack Transform

In this section we use the SST to derive a closed-form expression for the TD radiation pattern as an independent check for the TD multipole calculations. Referring to [5, eq. (10)], the TD radiation pattern (21) in the direction $\hat{\mathbf{r}}$ can be expressed as

$$\mathbf{F}(t;\ \hat{\mathbf{r}}) = \frac{-\mu}{4\pi} \iiint_V dV'\ \partial_t \mathbf{J}_{||}(\mathbf{r}',\ t + \hat{\mathbf{r}} \cdot \mathbf{r}'/c) \tag{34}$$

where $\mathbf{J}_{||} = \mathbf{J} - \hat{\mathbf{r}}(\hat{\mathbf{r}} \cdot \mathbf{J})$ and $\hat{\mathbf{r}}$ is the observation direction. The integral in (34) is termed the SST of $\mathbf{J}_{||}(\mathbf{r},\ t)$. Its physical interpretation is discussed in [5].

To calculate $\mathbf{J}_{||}$ for the present example we note that the component of $\hat{\mathbf{x}}$ transverse to $\hat{\mathbf{r}}$ is $-\hat{\boldsymbol{\theta}}_x \sin\theta_x$, where θ_x is the angle of $\hat{\mathbf{r}}$ from $\hat{\mathbf{x}}$ and $\hat{\boldsymbol{\theta}}_x$ is a unit vector along the θ_x coordinate. They are given by $\sin\theta_x = \sqrt{1 - \sin^2\theta\cos^2\phi}$ and $\hat{\boldsymbol{\theta}}_x = (\hat{\boldsymbol{\phi}}\sin\phi - \hat{\boldsymbol{\theta}}\cos\theta\cos\phi)/\sin\theta_x$. Equation (34)

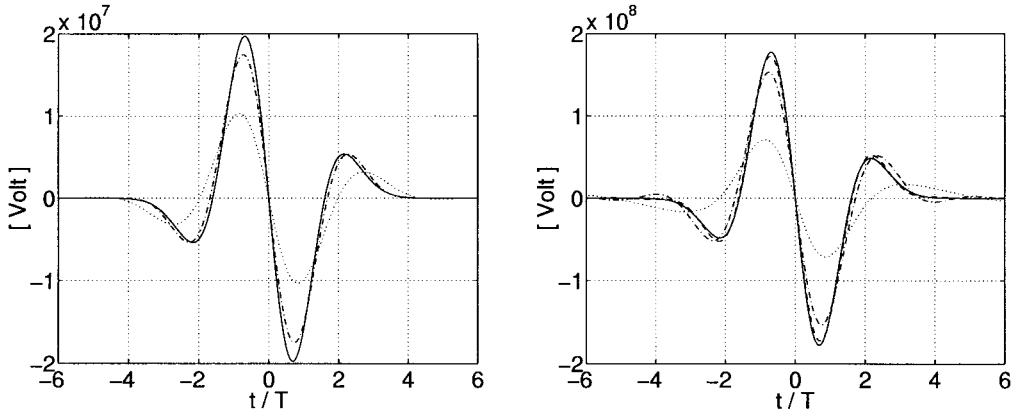

(a) (b)

Fig. 5. The TD radiation pattern $\mathbf{F}$ at $\theta = 0$ versus the normalized time τ/T. (a) and (b): "small" and "large" disks with $a/cT = 3$ and 9, respectively. In each figure, the dotted, dash-dotted and dashed lines depict, respectively, the waveforms obtained by summing the multipole series up to the $n = a/cT$ modes, up to the $n = 2a/cT$ mode, and up to the $n = 24$ mode. These results are compared with the exact SST result (37) (solid). For case (a), the $n = 24$ result coincides with the SST.

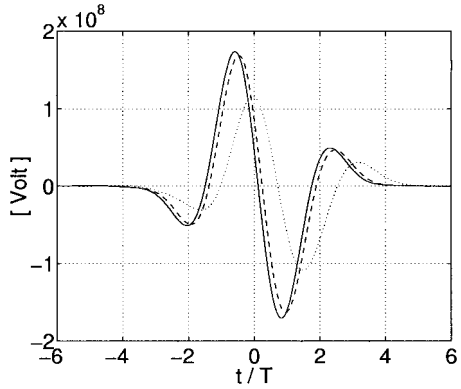

Fig. 6. The radiated waveforms along the z axis due to a current disk with $a = 9cT$ versus the normalized time τ/T. Dotted, dashed, and solid lines depict the waveforms at $z = 3a$, $9a$, and $18a$, respectively.

with (31) therefore becomes

$$\mathbf{F}(t;\hat{\mathbf{r}}) = \hat{\boldsymbol{\theta}}_x \sin\theta_x \frac{-\mu}{4\pi} f'(t) * \iiint_{r'<a} dV' \delta(z')\delta(t+\hat{\mathbf{r}}\cdot\mathbf{r}'/c) \tag{35}$$

where $f' \equiv \partial_t f$ and $*$ is a time convolution. The integral in (35), henceforth termed $D(t;\theta)$, is related to the TD effective height defined in [5, eq. (5)]. This integral reduces to the length of the line of intersection between the source disk on the $z = 0$ plane and the slanted plane $\hat{\mathbf{r}}\cdot\mathbf{r}' = -ct$ (Fig. 7). For a given t the distance of this line from the origin is $ct/\sin\theta$, hence, its length is $2\sqrt{a^2 - (ct/\sin\theta)^2}$, giving

$$D(t;\theta) = \frac{2c}{\sin\theta}\sqrt{a^2 - (ct/\sin\theta)^2}, \qquad \text{for } |ct| < a\sin\theta \tag{36}$$

and zero otherwise. This expression is the TD analog of the well known FD expression for the a radiation from a circular disk. However, unlike the FD analysis that involves spatial Fourier transforms and Bessel functions followed by frequency transform into the TD, the TD analysis above involves only a geometrical projection of the source disk. In particular, for $\theta \to 0$: $D(t;\theta) \to \pi a^2 \delta(t)$ and $\theta_x = \pi/2$, giving

$$\mathbf{F}(t)|_{\theta=0} = -\hat{\mathbf{x}}(\mu/4\pi)\pi a^2 f'(t). \tag{37}$$

This result is used in Fig. 5 to verify the result of the multipole expansion. As noted earlier, full agreement is obtained provided that one takes a sufficient number of multipoles.

V. Concluding Remarks

We presented a TD multipole expansion of the electromagnetic field radiated by a pulsed source distribution of finite support. The formulation has been based on the TD spherical transmission line representation, which can be applied to any spherically stratified medium of any conical cross section, but explicit expressions have been derived only for radiation in free-space. The spherical transmission line formulation describes the TD field and energy transmission mechanisms in a physically transparent fashion which will be utilized in a companion paper [1] to define and explore the TD energy concepts such as TD reactive energy and Q.

The final expression for the field have been expressed explicitly in terms of the TD multipole moments, which are calculated from the TD current distribution via (22). The TD multipole functions may be found, alternatively, from measurements of the TD field distribution [see, e.g., (23)]. Bounds on the convergence and on the number of the relevant terms have been established in Section III-D. In particular, it has been shown that the near-zone field consists of strong reactive constituents, but they are practically confined within the TD Fresnel zone [see (30)]. Bounds on the reactive fields have also been established there.

Finally, we demonstrated the TD multipole expansion through a numerical example of pulsed radiation from a circular current disk. We calculate the TD multipole moment functions and demonstrated that the number of relevant spherical modes is governed by the ratio a/cT between the source size a and the pulse length T. To check the validity of the calculations we compared the TD radiation pattern obtained via this approach with the closed-form expression

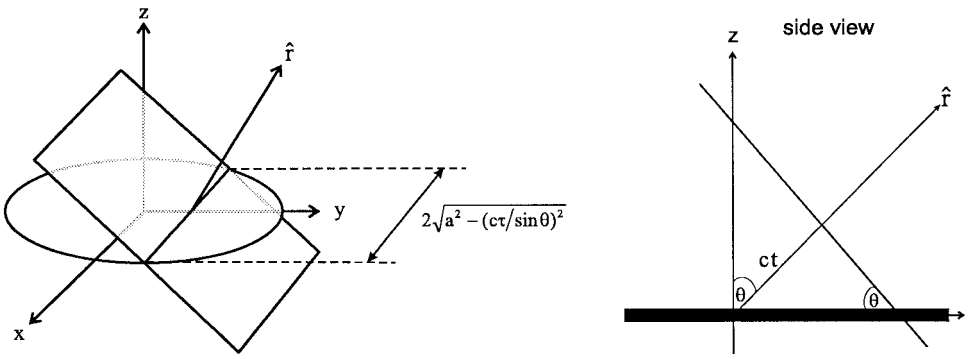

Fig. 7. Geometrical interpretation of the SST integration. (a) Front view. (b) Side view.

in (36) obtained independently via the SST approach of [5]. Further analysis of this example from an energy perspective will be presented in [1].

APPENDIX
RELATION TO THE FREQUENCY-DOMAIN EXPANSION

In this section, we briefly summarize the generalized spherical transmission line representation for time harmonic fields [17, secs. 2.5–2.7], which is recast here in a format that can readily be extended to the TD. No special symbols are used to denote the FD field constituents, which have a suppressed time-dependence $e^{j\omega t}$.

A. Spherical Transmission Line Formulation

Following [17, eq. (2.5.8)], the time-harmonic field in the spherical configuration of Fig. 1 can be described as a superposition of spherical modes of the form (1) and (2), where the transverse mode functions are found via the eigenfunction analysis of Section III. The modal amplitudes $V_\nu^\alpha(r)$ and $I_\nu^\alpha(r)$ are described most systematically by the first-order transmission line equations [17, eq. (2.5.9)]. However, since in this formulation ω appears implicitly inside square roots, here we use the wave equations whose form is more amenable for transformation into the TD. The principal amplitude functions for the E and H modes, I_ν^e and V_ν^h, respectively, satisfy the spherical wave equations

$$\left[\epsilon\frac{d}{dr}\epsilon^{-1}\frac{d}{dr}+k^2-\frac{k_{t\nu}^{e2}}{r^2}\right]I_\nu^e=j\omega\epsilon v_\nu^e-\epsilon\frac{d}{dr}\frac{i_\nu^e}{\epsilon} \tag{38a}$$

$$\left[\mu\frac{d}{dr}\mu^{-1}\frac{d}{dr}+k^2-\frac{k_{t\nu}^{h2}}{r^2}\right]V_\nu^h=j\omega\mu i_\nu^h. \tag{38b}$$

Noting that $k_{t\nu}^h$ are independent of r and ω, these equations are readily transformed into the TD equations in (38). The other two amplitude functions are determined from their solutions via

$$I_\nu^h=\frac{-1}{j\omega\mu}\frac{d}{dr}V_\nu^h,\qquad V_\nu^e=\frac{-1}{j\omega\epsilon}\left(\frac{d}{dr}I_\nu^e+i_\nu^e\right). \tag{39}$$

The transmission line source functions $v_\nu^\alpha(r)$ and $i_\nu^\alpha(r)$ in (38) are obtained by projecting the source distribution $\mathbf{J}(\mathbf{r})$ on the transversal mode functions as shown in (8).

For the problem of radiation in free-space $k_{t\nu}^\alpha$ is given in (9). The solution of the spherical wave equations (38) for $r>a$ (outside the source region) can be expressed as

$$\begin{Bmatrix} I_\nu^e(r)\\ V_\nu^h(r)\end{Bmatrix}=krh_n^{(2)}(kr)M_\nu^{e,h}(\omega) \tag{40}$$

where $h_n^{(2)}$ are the spherical Bessel functions [18], and M_ν^α are constant to be derived below. The associated amplitudes obtained via (39) are

$$\begin{Bmatrix} V_\nu^e(r)\\ I_\nu^h(r)\end{Bmatrix}=j\eta^{\pm1}M_\nu^{e,h}(\omega)\frac{d}{dr}\left[rh_n^{(2)}(kr)\right]. \tag{41}$$

In order to transform these solutions into the TD, we use (see [18, eq. (10.1.17)]) $h_n^{(2)}(x)=-j^ne^{-jx}\sum_{l=0}^n a_{n,l}(jx)^{-l-1}$, where $a_{m,l}$ are given after (14) to rewrite (40) as

$$\begin{Bmatrix} I_\nu^e(r)\\ V_\nu^h(r)\end{Bmatrix}=j^{n+1}e^{-jkr}\sum_{l=0}^n a_{n,l}(jkr)^{-l}M_\nu^\alpha(\omega). \tag{42}$$

The final result in (13) is obtained by transforming this expression into the TD, using

$$M_\nu^\alpha(t)=\frac{1}{2\pi}\int_{-\infty}^{\infty}d\omega\, e^{j\omega t}j^{n+1}M_\nu^\alpha(\omega). \tag{43}$$

Note that the transformation from (42) to (13) utilizes the small ω behavior $M_\nu^\alpha(\omega)\sim\omega^{N^\alpha}$ with N^α defined in (18), which follows from (46) and (47) by using $j_n(x)\sim x^n/(2n+1)!!$.

B. Calculation of the Multipole Moments

Consider the E mode first, we note from (8) that the source term in (38) is given by

$$\begin{aligned} q(r)&=-j\omega\epsilon v_\nu^e+\frac{d}{dr}i_\nu^e\\ &=\oiint d\Omega\left[J_rk_{t\nu}^e\Phi_\nu^e+\frac{d}{dr}(r\mathbf{J}\cdot\mathbf{e}_\nu^e)\right]. \end{aligned} \tag{44}$$

Next, we express the solution of (38) as $I_\nu^e(r)=\int_0^a dr' g_n(r,r')q(r')$ where the Green's function of (38) is $g_n(r,r')=jkrr'j_n(kr_<)h_n^{(2)}(kr_>)$ with $r_{\lessgtr}=\min_{\max}\{r,r'\}$. We thus identify in (40) $M_\nu^e(\omega)=j\int_0^a dr\, rj_n(kr)q(r)$ and, from (44)

$$M_\nu^e(\omega)=j\int_0^a dr\, rj_n(kr)\oiint d\Omega[\mathbf{J}\cdot\hat{\mathbf{r}}k_{t\nu}^e\Phi_\nu+\partial_r(r\mathbf{J}\cdot\mathbf{e}_\nu^e)]. \tag{45}$$

Using the identity $\hat{\mathbf{r}}j_n(kr)k_{t\nu}^e\Phi_\nu=k_{t\nu}^e r\nabla\times\nabla\times[\mathbf{r}j_n(kr)\Phi_\nu]+\partial_r[rj_n(kr)]\mathbf{e}_\nu^e$ and collecting terms we

obtain

$$M_\nu^e(\omega) = \frac{j}{k_{t\nu}^e} \iiint_V dV\, \mathbf{J} \cdot \nabla \times [\mathbf{r} j_n(kr) \mathbf{h}_\nu^e] + j \int_0^a dr \oiint d\Omega\, \partial_r \mathbf{e}_\nu^e \cdot [r^2 j_n(kr) \mathbf{J}].$$

The last integral yields

$$\oiint d\Omega\, r^2 j_n(kr) \mathbf{J} \cdot \mathbf{e}_\nu^e|_{r=a^+} = 0$$

and, thus, we end up with

$$M_\nu^e(\omega) = j \iiint_V dV \mathbf{J} \cdot \nabla \times [j_n(kr) \mathbf{h}_\nu^e] = j \iiint_V dV j_n(kr) \mathbf{h}_\nu^e \cdot \nabla \times \mathbf{J} \tag{46}$$

where in getting to the last expression we rewrite the integrand of the first one as $\mathbf{J} \cdot \nabla \times [j_n(kr)\mathbf{h}_\nu^e] = j_n(kr)\mathbf{h}_\nu^e \cdot \nabla \times \mathbf{J} - \nabla \cdot [\mathbf{J} \times j_n(kr)\mathbf{h}_\nu^e]$ and then note that the volume integration of the divergence reduces to a surface integration over the envelope of V whereon $\mathbf{J}$ vanishes.

For the H mode we use (8b) to express the source term in (38) as

$$q(r) = -j\omega\mu i_\nu^h(r) = \frac{-j\omega\mu}{k_{t\nu}^h} \oiint d\Omega\, \mathbf{J} \cdot [\hat{\mathbf{r}} \times {}_t\nabla \Phi_\nu].$$

Noting from (4) that $\mathbf{e}_\nu^h = (k_{t\nu}^h)^{-1} \hat{\mathbf{r}} \times {}_t\nabla \Phi_\nu^h$ and proceeding as above we obtain

$$M_\nu^h(\omega) = k\eta \iiint_V dV\, \mathbf{J} \cdot [j_n(kr) \mathbf{e}_\nu^h]. \tag{47}$$

Equations (46) and (47) are similar to those given in the literature (e.g., [19, eq. 4.18]), which were calculated directly from Maxwell's equation without recourse to the transmission line procedure.

The TD expressions for $M_\nu^\alpha(t)$ are obtained by using in (46) and (47) $j_n(z) = (2n!)^{-1}(z/2)^n \int_{-1}^1 d\xi (1-\xi^2)^n e^{jz\xi}$ (see [18, eq. (9.1.20)]), giving

$$j^{n+1} M_\nu^e(\omega) = \frac{-1}{2n!} \left(\frac{j\omega}{2c}\right)^n \iiint_V dV [\nabla \times \mathbf{J}] \cdot \left[\mathbf{h}_\nu^e r^n \int_{-1}^1 d\xi (1-\xi^2)^n e^{jkr\xi}\right] \tag{48a}$$

$$j^{n+1} M_\nu^h(\omega) = \frac{\eta}{n!} \left(\frac{j\omega}{2c}\right)^{n+1} \iiint_V dV\, \mathbf{J} \cdot \left[\mathbf{e}_\nu^h r^n \int_{-1}^1 d\xi (1-\xi^2)^n e^{jkr\xi}\right]. \tag{48b}$$

These expressions can be inverted to the TD via (43), giving the final results in (22).

REFERENCES

[1] A. Shlivinski and E. Heyman, "Time-domain near field analysis of short pulse antennas—Part II: Reactive energy and the antenna Q," *IEEE Trans. Antennas Propagat.*, this issue, pp. 280–286.

[2] B. Z. Steinberg, E. Heyman, and L. B. Felsen, "Phase space beam summation for time dependent radiation from large apertures: Continuous parametrization," *J. Opt. Soc. Amer. A*, vol. 8, pp. 943–958, 1991.

[3] T. B. Hansen and A. D. Yaghjian, "Planar near field scanning in the time domain—Part I: Formulation," *IEEE Trans. Antennas Propagat.*, vol. 42, pp. 1280–1291, Sept. 1994; "Part II: Sampling theorem and computation schemes," vol. 42, pp. 1292–1300, Sept. 1994.

[4] E. Heyman, "Time-dependent plane-wave spectrum representations for radiation from volume source distributions," *J. Math. Phys.*, vol. 37, pp. 682–692, 1996.

[5] A. Shlivinski, E. Heyman, and R. Kastner, "Antenna characterization in the time domain," *IEEE Trans. Antennas Propagat.*, vol. 45, pp. 1140–1149, July 1997.

[6] R. F. Harrington, "On the gain and bandwidth of directional antennas," *IRE Trans. Antennas Propagat.*, vol. AP-6, pp. 219–225, July 1958.

[7] R. E. Collin and S. Rothschild, "Evaluation of antenna Q," *IRE Trans. Antennas Propagat.*, vol. AP-12, pp. 23–27, Jan. 1964.

[8] R. L. Fante, "Quality factor of general ideal antennas," *IEEE Trans. Antennas Propagat.*, vol. AP-17, pp. 151–155, 1969.

[9] J. E. Hansen, *Spherical Near-Field Antenna Measurements.* London, U.K.: Peter Peregrinus, 1988.

[10] D. M. Grimes and C. A. Grimes, "Power in modal radiation: Limitations of the complex Poynting theorem and potential for electrically small antenna," *J. Electromagn. Wave Applicat.*, vol. 11, pp. 1741–1746, 1997.

[11] W. C. Davidon, "Time-dependent multipole analysis," *J. Phys. A: Math., Nucl. General*, vol. 6, pp. 1635–1646, 1973.

[12] W. B. Campbell, J. Mack, and T. A. Morgan, "Relativistic time-dependent multipole analysis for scalar, electromagnetic, and gravitational fields," *Phys. Rev. D*, vol. 15, pp. 2156–3164, 1977.

[13] E. Heyman and A. J. Devaney, "Time dependent multipoles and their application for radiation from volume source distributions," *J. Math. Phys.*, vol. 37, pp. 682–692, 1996.

[14] O. M. Buyukaura and S. S. Koc, "Two alternative expressions for the wave expansion of time domain scalar free-space Green's function and an application: Scattering by a soft sphere," *J. Acoust. Soc. Amer.*, to be published.

[15] T. B. Hansen and A. D. Yaghjian, "Spherical expansions of time-domain acoustic fields: Application to near field scanning," *J. Acoust. Soc. Amer.*, vol. 98, pp. 1204–1213, 1995.

[16] T. B. Hansen, "Formulation of spherical near-field scanning for electromagnetic fields in the time-domain," *IEEE Trans. Antennas Propagat.*, vol. 45, pp. 620–630, Apr. 1997.

[17] L. B. Felsen and N. Marcuvitz, *Radiation and Scattering of Waves.* Englewood Cliffs, NJ: Prentice Hall, 1973.

[18] M. Abramowitz and I. A. Stegun, *Handbook of Mathematical Functions.* New York: Dover, 1972.

[19] A. J. Devaney and E. Wolf, "Multipole expansions and plane wave representations of the electromagnetic field," *J. Math. Phys.*, vol. 15, pp. 234–244, 1974.

[20] E. Heyman and T. Melamed, "Certain consideration in aperture synthesis for ultra-wideband/short-pulsed fields," *IEEE Trans. Antennas Propagat.*, vol. 42, pp. 518–525, Apr. 1994.

Amir Shlivinski was born in Tel-Aviv, Israel, in February 1969. He received the B.Sc. (*cum laude*) and the M.Sc. (*summa cum laude*) degrees in electrical engineering, both from Tel-Aviv University, Israel, in 1991 and 1997, respectively. He is currently working toward the Ph.D. degree at the same university.

His main fields of interest are electromagnetic and antenna theory, wave theory, and time-domain phenomena.

E. Heyman (S'80–M'82–SM'88), for a biography, see p. 528 of the May 1995 issue of this TRANSACTIONS.